A model for droplet heating and its implementation into ANSYS Fluent

O. Rybdylova[a,*], M. Al Qubeissi[a,b], M. Braun[c], C. Crua[a], J. Manin[d], L.M. Pickett[d], G. de Sercey[a], E.M. Sazhina[a], S.S. Sazhin[a], M. Heikal[a]

[a] *Sir Harry Ricardo Laboratories, School of Computing, Engineering and Mathematics, University of Brighton, Brighton BN2 4GJ, United Kingdom*
[b] *Centre for Mobility & Transport, School of Mechanical, Aerospace and Automotive Engineering, Coventry University, Coventry CV1 2JH, United Kingdom*
[c] *ANSYS Germany GmbH, Darmstadt 64295, Germany*
[d] *Sandia National Laboratories, 7011 East Avenue, 94550 Livermore, CA, United States of America*

Abstract

The main ideas of the model for droplet heating and evaporation, based on the analytical solution to the heat conduction equation inside the droplet, and its implementation into ANSYS Fluent are described. The model is implemented into ANSYS Fluent using User-Defined Functions (UDF). The predictions of ANSYS Fluent with the new model are verified against the results predicted by in-house research code for an n-dodecane droplet heated and evaporated in hot air. Also, the predictions of this version of ANSYS Fluent are compared with in-house experimental data.

Keywords: Droplets, Heating, Evaporation, ANSYS Fluent, Diesel fuel, n-dodecane

Nomenclature

$B_M,\ B_T$	Spalding mass and heat transfer numbers
c_p	specific heat capacity at constant pressure
D	binary diffusivity coefficient of vapour in air
h	convection heat transfer coefficient

*Corresponding author
Email address: O.Rybdylova@brighton.ac.uk (O. Rybdylova)

I_n	integrals, used in series (2) and (6)
j	parameter, defined in (4c)
k	thermal conductivity
L	latent heat of evaporation
m	mass
$\dot{m}$	evaporation rate
M	molar mass
N_L	number of layers inside a droplet
Nu	Nusselt number
Pe	Peclet number
p	pressure
Pr	Prandtl number
q	heat flux
r	radial coordinate from the centre of the droplet
R_d	radius of a droplet
Re	Reynolds number
Sc	Schmidt number
Sh	Sherwood number
t	time
T	temperature
$\mathbf{v}$	velocity
Y	mass fraction
x	molar fraction

Greek symbols

κ	parameter defined by (4b)
λ_n	eigenvalues
μ	dynamic viscosity
ρ	density
ϕ	parameter defined by Equation (5e)
χ	correction function defined by Equation (4c)
ζ	parameter defined by (4b)

Subscripts

d	droplet
eff	effective
g	gas
int	internal

l	liquid
ref	reference value
s	surface of droplet
sat	saturation
t	total
v	vapour
0	value at the beginning of a time step
∞	value in the far field

1. Introduction

A new model for multi-component droplet heating and evaporation, based on the analytical solutions to the heat transfer and species diffusion equations, has been developed by our group (see [1, 2] for the details). This model has been validated based on the available experimental data and the predictions of the numerical codes using the analytical solution to these equations [3, 4].

In the current study the analysis is restricted to mono-component droplets. The main ideas of the new model and the results of its implementation into the commercial CFD code ANSYS Fluent, via user-defined functions (UDF), macros, supported by ANSYS Fluent, are summarised. The results of the implementation of the model are compared with the predictions of the in-house code and validated against in-house experimental data.

The mathematical formulation and the implementation of the model are described in Section 2. In Section 3.1, the predictions of ANSYS Fluent with the new model are verified against the predictions of the in-house code. In Section 3.2, the experimental set up is described, and the results of simulations are compared with the experimental data. The main results of the paper are summarised in Section 4.

2. Formulation of the problem

In the conventional approach, used in most available CFD codes, including ANSYS Fluent, droplet heating is modelled based on the solution to the following energy balance equation:

$$c_{pl} m_d \frac{dT}{dt} = 2\pi \mathrm{Nu} k_g R_d \left(T_g - T_s\right) + L\dot{m}_d + q_{\mathrm{int}}, \qquad (1)$$

where c_{pl} is droplet liquid specific heat capacity, m_d and R_d are droplet mass and radius, respectively, Nu is the Nusselt number, k_g is gas thermal conductivity, T_g and T_s are gas and surface temperatures, respectively, L is the latent heat of evaporation, q_{int} is heat supplied or removed from internal sources (e.g. chemical reactions). The derivation of this equation is based on the assumption that the effects of temperature gradients inside droplets can be ignored. This assumption is commonly supported by the fact that liquid thermal conductivity is much higher than gas thermal conductivity in most engineering applications. At the same time, when modelling transient processes this assumption should be based on the comparison of the liquid and gas thermal diffusivities and the values of the Fourier number. In most engineering applications, including Diesel engines, liquid thermal diffusivities are much lower than those of gas. This obviously brings into question the applicability of Equation (1). This equation cannot be used at all when the Fourier numbers are small.

In an alternative approach to the problem of droplet heating, taking into account the effects of temperature gradient inside droplets, the transient heat conduction inside the droplet is solved subject to the boundary conditions at the surface of the droplet. Assuming that all the processes inside the droplet are spherically symmetric, an analytical solution to this equation during any time step Δt ($t \in [0,\ \Delta t]$) has been found in the form [2, 4]:

$$T(r,t) = \frac{1}{r}\sum_{n=1}^{\infty}\left\{\left(I_n - \frac{R_d \sin\lambda_n}{\lambda_n^2}\zeta(0)\right)\frac{\exp\left(-\kappa\lambda_n^2 t\right)}{b_n} - \right.$$
$$\left. - \frac{R_d \sin\lambda_n}{b_n\lambda_n^2}\int_0^t \frac{d\zeta(\tau)}{d\tau}\exp\left(-\kappa\lambda_n^2(t-\tau)\right)d\tau\right\}\sin\left(\lambda_n\frac{r}{R_d}\right) + T_{\text{eff}}(t), \quad (2)$$

where λ_n are positive roots to the eigenvalue equation

$$\lambda\cos\lambda + j\sin\lambda = 0; \quad (3)$$

in ascending order,

$$b_n = \frac{1}{2}\left(1 + \frac{j}{j^2+\lambda_n^2}\right),\ I_n = \int_0^{R_d}\frac{r}{R_d}T_0(r)\sin\left(\lambda_n\frac{r}{R_d}\right)dr,$$

$T_0(r)$ is the initial temperature distribution inside the droplet or the distribution predicted at the previous time step;

$$\kappa = \frac{k_{\text{eff}}}{c_{pl}\rho_l R_d^2},\ \zeta(t) = \frac{hT_{\text{eff}}(t)\,R_d}{k_{\text{eff}}},\ T_{\text{eff}} = T_g + \frac{\dot{m}_d L}{2\pi R_d \text{Nu} k_g}; \tag{4a}$$

$$j = \frac{hR_d}{k_{\text{eff}}} - 1,\ h = \frac{k_g \text{Nu}}{2R_d},\ k_{\text{eff}} = \chi k_l,\ \chi = \left(1.86 + 0.86\tanh\left(2.225\lg\frac{\text{Pe}}{30}\right)\right), \tag{4b}$$

$$\text{Pe} = 0.79\left|\mathbf{v}_g - \mathbf{v}_d\right|\frac{\mu_g}{\mu_l}\frac{\text{Re}_d^{1/3}}{1+B_M}\frac{\rho_l R_d c_{pl}}{k_l},\ \text{Re}_d = \frac{2R_d\rho_g\left|\mathbf{v}_g - \mathbf{v}_d\right|}{\mu_g}, \tag{4c}$$

where $B_M = (Y_{vs} - Y_{v\infty})/(1 - Y_{vs})$, $Y_{v\infty}$ and Y_{vs} are mass fractions of vapour in the ambient gas and at the droplet surface. Note that

$$Y_{vs} = \frac{x_{vs}M_v}{x_{vs}M_v + (1 - x_{vs})M_a},\ x_{vs} = \frac{p_{sat}}{p}.$$

The Nusselt number is approximated as [2]:

$$\text{Nu} = \frac{\ln(1+B_T)}{B_T}\text{Nu}^*, \tag{5a}$$

$$\text{Nu}^* = 2 + \frac{(1+\text{Re}_d\text{Pr})^{1/3}\max\left(1, \text{Re}_d^{0.077}\right) - 1}{F(B_T)}, \tag{5b}$$

$$\text{Sh}^* = 2 + \frac{(1+\text{Re}_d\text{Sc})^{1/3}\max\left(1, \text{Re}_d^{0.077}\right) - 1}{F(B_M)}, \tag{5c}$$

$$F(B_T) = (1+B_T)^{0.7}\frac{\ln(1+B_T)}{B_T},\ B_T = (1+B_M)^{\phi} - 1, \tag{5d}$$

$$\phi = \frac{c_{pv}\rho_g D}{k_g}\frac{\text{Sh}^*}{\text{Nu}^*},\ \text{Pr} = \frac{c_{pg}\mu_g}{k_g},\ \text{Sc} = \frac{\mu_g}{\rho_g D}. \tag{5e}$$

The term $R_d \sin\lambda_n / (b_n\lambda_n^2)\int_0^t d\zeta(\tau)/d\tau\ \exp\left(-\kappa\lambda_n^2(t-\tau)\right)d\tau$ was shown to be negligibly small. This allowed us to simplify Expression (2) to:

$$T(r,t) = \frac{1}{r}\sum_{n=1}^{\infty}\left\{\left(I_n - \frac{R_d\sin\lambda_n}{\lambda_n^2}\zeta(0)\right)\frac{\exp\left(-\kappa\lambda_n^2 t\right)}{b_n}\right\}\sin\left(\lambda_n\frac{r}{R_d}\right) + T_{\text{eff}}(t) \tag{6}$$

Droplet evaporation rate is estimated as [5]:

$$\dot{m}_d = -2\pi R_d D\rho_g \ln(1+B_M)\,\text{Sh}^*. \tag{7}$$

3. Results and discussions

Equation (7) was solved using the customised version of ANSYS Fluent; the right-hand side of this equation was calculated by the UDF. Thermodynamic parameters of a droplet were calculated based on the average temperature inside the droplet, which was calculated using Simpson's method [6]. Gas parameters in the vicinity of the droplet surface were calculated based on reference temperature: $T_{\text{ref}} = (2T_s + T_g)/3$. The roots to Equation (3) were found using the bisection method with absolute accuracy of 10^{-8}; in simulations, we used 44 eigenvalues to calculate the series in (6).

The results predicted by ANSYS Fluent were verified against predictions made by the in-house code [4] (see Section 3.1) and then compared with experimental data (Section 3.2).

3.1. Verification of the results

The verification was performed based on the analysis of heating and evaporation of an n-dodecane droplet of 10 μm in radius with initial temperature of 300 K, uniform inside the droplet. The droplet was injected into quiescent air with $T_a = 650$ K, $p_a = 101325$ Pa. The mass fraction of vapour away from the droplet was assumed to be negligible. The thermodynamic properties of n-dodecane were taken from [7]. The reference values were obtained using the in-house code [4]. This code, in its turn, was verified using the in-house code based on the analytical solution to the heat transfer equation inside the droplet (see [4] for the details). The droplet volume was discretised into $N_L = 500$ concentric layers, $\delta t = 10^{-6}$ s; the reference value for the evaporation time was taken equal to $2.78 \cdot 10^{-3}$ s.

Simulations using the built-in heating and evaporation model of ANSYS Fluent, Discrete Phase Model (DPM), showed that in this model the effect of droplet evaporation on droplet heating is overestimated. This resulted in low droplet temperature at the end of evaporation and high error in the prediction of evaporation time.

Relative errors in the evaporation times for a number of simulations of ANSYS Fluent + UDF with various δt and N_L are summarised in Table 1; 'large k_l' corresponds to the case when droplet liquid thermal conductivity is set 1000 times higher in order to simulate the case of uniform temperature distribution inside a droplet. n-Dodecane properties were introduced to ANSYS Fluent simulations via polynomial definition and DEFINE_DPM_PROPERTY UDFs. Case 1 corresponds to ANSYS Fluent + UDF simulations based on

$N_L \setminus \delta t$, s	10^{-4}	10^{-5}	10^{-6}
500	$1.1 \cdot 10^{-2}$ (case 1)	$7.2 \cdot 10^{-3}$	$7.2 \cdot 10^{-3}$
100	$1.1 \cdot 10^{-2}$	$7.2 \cdot 10^{-3}$	$7.2 \cdot 10^{-3}$
50	$1.1 \cdot 10^{-2}$	$7.2 \cdot 10^{-3}$	$7.2 \cdot 10^{-3}$
10	N/A	$4.7 \cdot 10^{-2}$	$4.3 \cdot 10^{-2}$
4	N/A	N/A	$2.9 \cdot 10^{-2}$ (case 2)
large k_l	$9 \cdot 10^{-3}$ (case 3)	$7.2 \cdot 10^{-3}$	$6.5 \cdot 10^{-2}$

Table 1: Relative errors of evaporation time predicted by ANSYS Fluent + UDF relative to the reference value of $2.78 \cdot 10^{-3}$ s, obtained using the in-house code [4].

$N_L = 500$, $\delta t = 10^{-6}$ s; case 2: $N_L = 4$, $\delta t = 10^{-4}$ s; case 3: 'large k_l', $N_L = 100$, $\delta t = 10^{-6}$ s. As follows from Table 1, δt has a greater impact on the prediction of evaporation time than N_L. The smaller time step corresponds to the smaller values of the residuals; in most cases, $\delta t = 10^{-4}$ s leads to sufficiently accurate results. In three cases, denoted as 'N/A' in the table, the calculations did not converge; these correspond to coarse meshing. Overall, the results predicted by ANSYS Fluent + UDF based on (6) lead to errors of 1 – 5 %, depending on N_L value. One per cent error at $N_L = 500$ might be related to a different method of calculating integrals and eigenvalues (see Section 2 for the details) from the one used in the in-house code [4]. The results of the reference and ANSYS Fluent + UDF simulations for cases 1 and 2 are presented in Figures 1 and 2. The time evolutions of droplet radii as predicted by ANSYS Fluent and in-house code are shown in Figure 1a; Figures 1b and 2 show the evolutions of the average droplet temperature, temperatures in the centre, and at the surface of the droplet.

As follows from Figures 1 and 2, the process of droplet heating and evaporation is modelled by ANSYS Fluent + UDF with satisfactory accuracy. The droplet radius increases at the initial stage due to swelling and then decreases due to evaporation. Note that no equations were added to the UDF in order

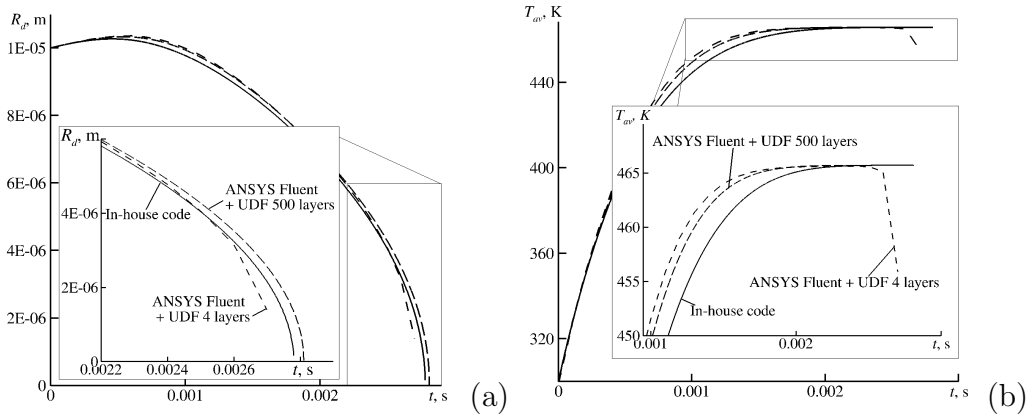

Figure 1: n-Dodecane droplet heating and evaporation. Initial droplet temperature is 300 K, temperature of air is 650 K: (a) evolution of the droplet radius; (b) evolution of the droplet average temperature. Solid curves – in-house code, long dashed curves – case 1, dashed curves – case 2.

to model droplet swelling: this is done using built-in ANSYS Fluent procedures, which take into account temperature-dependent density. In case 1, the predicted droplet temperatures increase monotonically; while in case 2, the droplet temperature drops slightly at the end of the evaporation process. This effect is believed to be related to the fact that the integrals I_n in (6) are calculated using coarse mesh (4 layers). The same effect takes place in the case of $N_L = 10$, and leads to higher errors or non-converging calculations (see Table 1). This should be taken into account when modelling a large number of droplets using ANSYS Fluent + UDF with coarse meshing inside droplets.

As follows from Figure 2, the difference between temperatures at the droplet centre and at the droplet surface is high. This effect is ignored in conventional CFD calculations of droplet heating and evaporation in fuel spray modelling. The case of 'large k_l' refers to uniform temperature distribution. As follows from Table 1, this does not have a big impact on evaporation time in the case considered. The average droplet temperature is also predicted with satisfactory accuracy (see Figure 3a). However, the errors in predicted temperatures at the droplet centre are high (about 20 K) (see Figure 3b). This behaviour is consistent with previous observations [8].

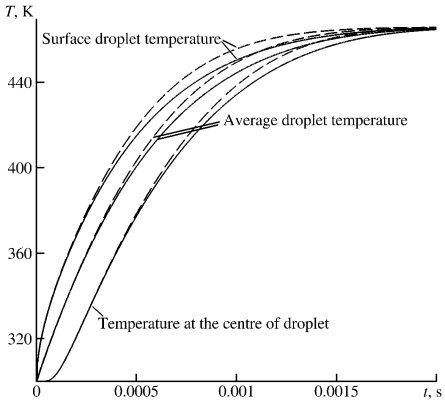

Figure 2: n-Dodecane droplet heating and evaporation. Initial droplet temperature is 300 K, temperature of air is 650 K: evolutions of the temperatures in the centre of the droplet, at the droplet surface, and of the average temperature. Solid curves – in-house code, long dashed curves – case 1.

3.2. Comparison of the model with experimental data

Experiments were conducted using a preburn combustion vessel [9]. This constant-volume chamber is of cubic shape, offering six faces that can be fitted with transparent sapphire windows or metal ports. The thermodynamic conditions simulated inside the chamber are achieved after combustion of a preburn mixture of combustible gases composed of C_2H_2, H_2, N_2 and O_2. After the spark-ignited preburn combustion, the internal temperature and pressure conditions decrease due to heat transfer to the vessel walls during a cool-down period of several seconds. The fuel is injected when the desired ambient conditions are reached during the cool-down.

Sprays of n-dodecane were injected at a pressure of 50 MPa into a quiescent gas mixture, $T_g = 707$ K, $p_g = 6.16$ MPa, using a commercial common-rail solenoid-actuated injector equipped with a single-hole nozzle. The axially-drilled orifice located at the tip of the nozzle was of 0.180 mm diameter and featured a converging conical shape (KS 1.5). We selected a single-hole axially-drilled nozzle to ensure that the fuel spray would develop along the centre of the combustion vessel, where the thermodynamic conditions are best controlled. The fuel injector was temperature-controlled to ensure that the state of the fuel prior to injection was known, with a target temperature of 363 K. The nozzle's temperature was measured using a dummy injector fitted with a thermocouple. This thermocouple was used to adjust the injector cooling system, as described in [10]. For these operating conditions

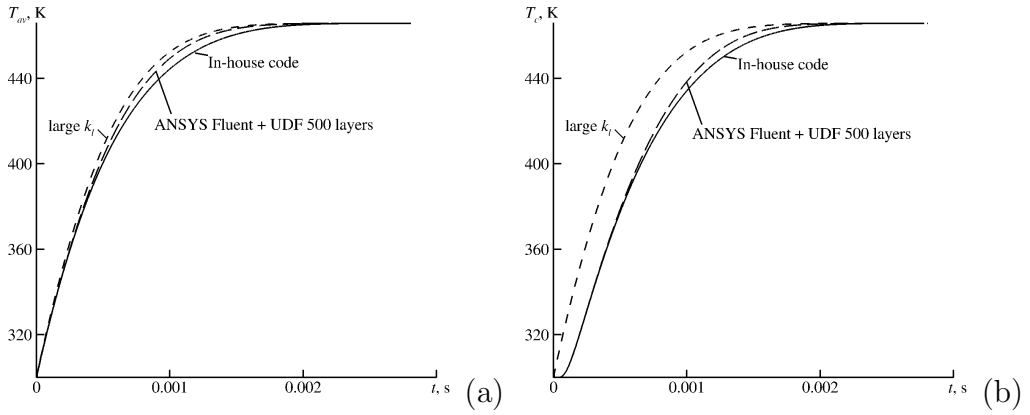

Figure 3: n-Dodecane droplet heating and evaporation. Initial droplet temperature is 300 K, temperature of air is 650 K: (a) evolution of the droplet average temperature; (b) evolution of the temperature in the centre of the droplet. Solid curves – in-house code, long dashed curves – case 1, dashed curves – case 3.

the maximum heating of the fuel due to friction inside the nozzle orifice is estimated at 20 K [11], hence the actual fuel temperature at the nozzle exit is expected to be 370 ± 10 K.

The spray was back-illuminated through one sapphire window along a line of sight and imaged through another sapphire window on the other side. The optical system was composed of a long-working-distance microscope lens, a high-speed CMOS camera (Photron SA-X2) and purpose-built LED illumination [12]. Two individual droplets were tracked throughout the video sequence, and their sizes measured based on the image processing technique described in [13]. The uncertainties concerning the droplet formation time and the droplet diameter were estimated as ± 0.033 ms, and $\pm 10\%$, respectively. The gas phase velocity in the vicinity of the droplet could not be measured, hence the relative droplet velocity is not known. However we can estimate an upper limit for the relative velocity from the observation that these droplets were not showing any sign of vibrational breakup, hence the gaseous Weber number for these conditions should be less than unity. Based on this observation we estimate that the relative initial droplet velocity should be less than 3.5 m/s. The mass fraction of vapour away from the droplets could not be measured. A steady-state analysis of the entrainment of the surrounding gas into a single free spray shows that there is no significant backward flow of vaporised fuel into the near-nozzle region of the spray [14]. Furthermore, our measurements were performed at the end of injection,

when the entrainment of ambient gases into the jet increases significantly due to a strong entrainment wave, and the near-nozzle region becomes more fuel-lean than the steady jet [15, 16].

There were no observations of the initial stages of droplet heating and evaporation processes. Hence, the comparison shown below will allow us to identify similarities in trends between the model and experimental data (to perform functionality testing of the model), but not quantitative agreement between the prediction of the model and experimental data. Three parameters could be used to adjust the model within the uncertainties of the experimental data: initial droplet size (to take into account droplet swelling); the initial relative droplet velocities; and the droplet initial temperature ($360 - 380$ K).

A series of simulations were performed with various R_{d0} and T_{d0}, v_0. Some results and comparison between experimental data and numerical simulation are presented in Figure 4. Experimental data related to both droplets are shown by triangles. As follows from Figure 4, the initial droplet velocity strongly affects the droplet evaporation time. In numerical simulations, droplets were injected into quiescent hot gas with initial velocity of v_0. As droplets evaporated, their relative velocities rapidly relaxed to zero. In the case of the initial droplet velocity of $v_0 = 3.5$ m/s, at $t = 2.983 \cdot 10^{-3}$ s, its velocity reduced to $\sim 2.4 \cdot 10^{-2}$ m/s ($R_{d0} = 17.5$ μm and $T_{d0} = 360$ K). In experiments, droplets were entrained in the air flow with complex vortex structures, although these were not captured. The velocity magnitude was calculated with a good accuracy, however the comparison between the experimental and theoretical data for droplet velocities could not be performed. The initial droplet temperature also has an impact on the evaporation time, the difference between cases $T_0 = 360$ K and $T_0 = 380$ K being about 4%.

As one can see from Figure 4, the model predicts the same trends as observed in the experiments. It is not possible, however, to use these experimental data for the detailed validation of the model under consideration, compared with the conventional model based on the assumption that the liquid thermal conductivity is infinitely large. This is related both to the errors in experimental data and limitations of the model. The model is based on a number of simplifying assumptions (although some assumptions of the conventional model have been relaxed) and is not expected to be reliable for conditions close to the critical conditions considered in the experiments.

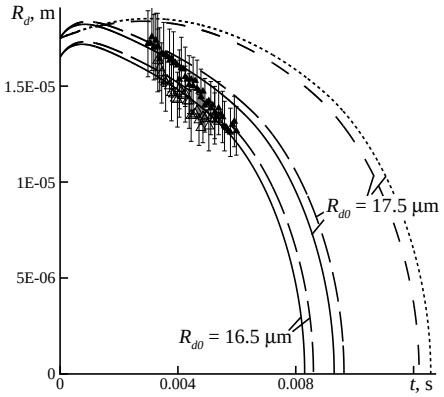

Figure 4: n-Dodecane droplet heating and evaporation. Experimental data vs ANSYS Fluent predictions. Triangles – experimental data: filled symbols – droplet 1, hollow symbols – droplet 2. Solid curves show theoretical predictions for $T_{d0} = 380$ K, $v_0 = 3.5$ m/s; long dashed curves – $T_{d0} = 360$ K, $v_0 = 3.5$ m/s; dashed curves – $T_{d0} = 380$ K, $v_0 = 0$ m/s; dotted curves – $T_{d0} = 360$ K, $v_0 = 0$ m/s.

4. Conclusion

The model for droplet heating and evaporation, based on the analytical solution to the heat conduction equation inside the droplet, has been implemented into ANSYS Fluent via User-Defined Functions (UDF). Predictions of n-dodecane droplet heating and evaporation using ANSYS Fluent with the new model have been shown to be noticeably different from, and better than, the predictions of the standard Fluent code, demonstrating the need to adopt this new modelling process. The customised version of Fluent has been verified by comparing results for an evaporating n-dodecane droplet with the prediction of the in-house research code. Also, the predictions of this version of Fluent have been compared with the trends of the in-house experimental data.

Acknowledgements

This work was supported by the UK's Engineering and Physical Science Research Council (grants EP/K005758/1, EP/M002608/1, EP/K020528/1). The experimental measurements were performed at the Combustion Research Facility, Sandia National Laboratories, Livermore, California, supported by the U.S. Department of Energy Office of Vehicle Technologies. Sandia is a

multiprogram laboratory operated by Sandia Corporation, a Lockheed Martin Company, for the United States Department of Energy's National Nuclear Security Administration under contract DE-AC04-94AL85000.

References

[1] S. S. Sazhin, Advanced models of fuel droplet heating and evaporation, Progress in Energy and Combustion Science 32 (2) (2006) 162 – 214. doi:10.1016/j.pecs.2005.11.001.

[2] S. S. Sazhin, Droplets and Sprays, Springer, 2014.

[3] S. S. Sazhin, A. Elwardany, P. Krutitskii, V. Deprédurand, G. Castanet, F. Lemoine, E. Sazhina, M. Heikal, Multi-component droplet heating and evaporation: Numerical simulation versus experimental data, International Journal of Thermal Sciences 50 (7) (2011) 1164 – 1180. doi:10.1016/j.ijthermalsci.2011.02.020.

[4] A. E. Elwardany, I. G. Gusev, G. Castanet, F. Lemoine, S. S. Sazhin, Mono- and multi-component droplet cooling/heating and evaporation: Comparative analysis of numerical models, Atomization and Sprays 21 (11) (2011) 907–931.

[5] B. Abramzon, W. Sirignano, Droplet vaporization model for spray combustion calculations, International Journal of Heat and Mass Transfer 32 (9) (1989) 1605 – 1618. doi:10.1016/0017-9310(89)90043-4.

[6] N. N. Kalitkin, Numerical methods, Nauka, 1978, [in Russian].

[7] B. Abramzon, S. S. Sazhin, Convective vaporization of a fuel droplet with thermal radiation absorption, Fuel 85 (1) (2006) 32 – 46. doi:10.1016/j.fuel.2005.02.027.

[8] S. S. Sazhin, T. Kristyadi, W. Abdelghaffar, M. Heikal, Models for fuel droplet heating and evaporation: Comparative analysis, Fuel 85 (1213) (2006) 1613 – 1630. doi:10.1016/j.fuel.2006.02.012.

[9] L. M. Pickett, C. L. Genzale, G. Bruneaux, L.-M. Malbec, L. Hermant, C. Christiansen, J. Schramm, Comparison of diesel spray combustion in different high-temperature, high-pressure facilities, SAE International Journal of Engines 3 (2) (2010) 156–181. doi:10.4271/2010-01-2106.

[10] M. Meijer, B. Somers, J. Johnson, J. Naber, S.-Y. Lee, L.-M. Malbec, G. Bruneaux, L. M. Pickett, M. Bardi, R. Payri, T. Bazyn, Engine Combustion Network (ECN): Characterization and comparison of boundary conditions for different combustion vessels, Atomization and Sprays 22 (9) (2012) 777–806. doi:10.1615/AtomizSpr.2012006083.

[11] A. Theodorakakos, G. Strotos, N. Mitroglou, C. Atkin, M. Gavaises, Friction-induced heating in nozzle hole micro-channels under extreme fuel pressurisation, Fuel 123 (2014) 143 – 150. doi:10.1016/j.fuel.2014.01.050.

[12] J. Manin, M. Bardi, L. M. Pickett, R. N. Dahms, J. C. Oefelein, Microscopic investigation of the atomization and mixing processes of diesel sprays injected into high pressure and temperature environments, Fuel 134 (2014) 531–543. doi:10.1016/j.fuel.2014.05.060.

[13] C. Crua, G. de Sercey, M. R. Heikal, Dropsizing of near-nozzle diesel and RME sprays by microscopic imaging, in: 12th ICLASS, Heidelberg, Germany, 2-6 Sep 2012.

[14] T. Fuyuto, Y. Hattori, H. Yamashita, M. Mashida, Backward flow of hot burned gas surrounding high-pressure diesel spray flame from multihole nozzle, SAE International Journal of Engines 9 (1). doi:10.4271/2015-01-1837.

[15] M. Musculus, K. Kattke, Entrainment waves in diesel jets, SAE International Journal of Engines 2 (1) (2009) 1170–1193. doi:10.4271/2009-01-1355.

[16] W. E. Eagle, M. Musculus, J. C. Oefelein, L.-M. Malbec, G. Bruneaux, Measuring transient entrainment rates of a confined vaporizing diesel jet, in: 26th ILASS Americas, Portland (OR), USA, May 2014.